Contrib Mineral Petrol (2004) 146: 606–619
DOI 10.1007/s00410-003-0517-3

ORIGINAL PAPER

Gregory M. Yaxley · Gerhard P. Brey

Phase relations of carbonate-bearing eclogite assemblages from 2.5 to 5.5 GPa: implications for petrogenesis of carbonatites

Received: 18 April 2003 / Accepted: 18 August 2003 / Published online: 9 October 2003

Abstract We have experimentally investigated the phase and melting relations of garnet + clinopyroxene + carbonate assemblages at 2.5–5.5 GPa, to assess the feasibility of carbonated eclogite as a source for some crustally emplaced carbonatites. The solidus of our composition was at ≈1,125 °C at 2.5 GPa, ≈1,225 °C at 3.5 GPa and ≈1,310 °C at 5.0 GPa. Melts were sodic calcio-dolomitic carbonatites, and were markedly more calcic than the dolomitic melts produced by partial melting of carbonated peridotite. Na contents of the experimental carbonatites decreased with increasing pressure when compared at similar degrees of melting, and SiO_2 contents increased with degree of melting. Experiments on a second composition with enhanced Na_2O demonstrated its strong effect in lowering melting temperatures in carbonate eclogite. Natural carbonated eclogite bodies in the peridotitic upper mantle will have a range of solidus temperatures. In many cases, carbonate will be molten in the upper ≥250 km. Carbonate melt would segregate from its source eclogite at very low melt fractions and infiltrate surrounding peridotitic wall rock. This would result in metasomatic enrichment of the peridotitic wall rock, but its exact nature will depend on the relative P–T positions of the eclogite + CO_2 and peridotite + CO_2 solidii. As a result of these inevitable metasomatic interactions, it is considered unlikely that carbonatite melts derived from carbonated eclogite in the upper mantle could be emplaced into the crust unmodified. However, they may have a role in metasomatically enriching and carbonating parts of the upper mantle, producing sources suitable for subsequent production of silica undersaturated silicate liquids and carbonatites ultimately emplaced in the crust.

Editorial responsibility: J. Hoefs

G. M. Yaxley (✉) · G. P. Brey
Institut für Mineralogie, Universität Frankfurt,
Senckenberganlage 28, 60054 Frankfurt/M, Germany
E-mail: Greg.Yaxley@anu.edu.au

Present address: G. M. Yaxley
Research School of Earth Sciences,
The Australian National University,
Canberra ACT 0200, Australia

Introduction

Crustally emplaced carbonatites are carbonate-rich and silica-poor magmatic rocks derived from the upper mantle and known from both continental and oceanic settings. Understanding their origins is important as they are often considered to be informative probes into the nature of mantle geochemistry because of their strong enrichments in most incompatible elements, which buffers them against crustal contamination, their wide-spread geographic and tectonic distribution and their variation in age (Bell and Tilton 2001). In addition, they have been shown to have an important role in metasomatic redistribution of chemical components in oceanic (Hauri et al. 1993) and continental (e.g. Yaxley et al. 1991; Rudnick et al. 1993) lithosphere, and may be responsible for enrichment in some ocean island basalt (OIB) sources (Nelson et al. 1988; Hauri et al. 1993).

Although there is consensus that melts parental to crustal carbonatites derive from partial melting in the mantle (Bell et al. 1982; Nelson et al. 1988; Deines 1989; Kwon et al. 1989), there is debate about the precise nature of these melts, the nature and location of their mantle sources and the processes that modify the parental melts before emplacement into the crust. Models include derivation of carbonatites by immiscibility of carbonate and silicate liquids from parental carbonated, silica-undersaturated melts (Koster van Groos and Wyllie 1973; Kjarsgaard and Hamilton 1988, 1989; Lee and Wyllie 1996; Lee and Wyllie 1997a, 1997b), by direct partial melting of carbonated upper mantle peridotite to produce dolomitic primary liquids (Wyllie and Huang 1975; Wallace and Green 1988; Sweeney 1994), or by fractional crystallisation of carbonated alkali silicate melts (Veksler et al. 1998).

Carbonatites and OIBs are strikingly similar in radiogenic isotope signatures. Furthermore, many carbonatites and OIBs exhibit the so-called HIMU isotopic signature, exhibiting high $^{238}U/^{206}Pb$, radiogenic Pb isotopes, low ϵ_{Nd}, high $^{87}Sr/^{86}Sr$ and high $^{187}Os/^{186}Os$ (Nelson et al. 1988; Tilton and Bell 1994; Bell 2001; Bell and Tilton 2001; Hoernle et al. 2002). This is generally interpreted to derive from ancient recycled oceanic crust in the source regions of these rocks. Thus, an alternative model for carbonatite genesis is that they form by partial melting of carbonate-bearing eclogite (Treiman and Essene 1983; Nelson et al. 1988; Hoernle et al. 2002) in the upper mantle. The carbonated eclogite is derived from altered oceanic crustal material, recycled back into the mantle by subduction, and stored for billions of years in the mantle, before incorporation into the carbonatites' source regions. If this is true, then carbonatites can potentially reveal important information about large-scale mantle dynamic processes and the evolution of the Earth's crust–mantle system.

A necessary condition for this model to be valid is that carbonate-bearing eclogite assemblages should be capable of yielding carbonatite melts at upper mantle pressures and temperatures. Accordingly, we have investigated the phase and melting relations of carbonate-bearing eclogite assemblages (garnet + clinopyroxene ± quartz/coesite) using high-pressure experimental techniques. We include data from an earlier investigation of compositions EC1 and EC2 (Yaxley 1999) conducted at 3.0 and 3.5 GPa, and present additional results from new experiments conducted at 2.5, 4.0, 4.3, 5.0 and 5.5 GPa.

Experimental procedures

Choice and preparation of compositions

The compositions EC1 and EC2 were used in these experiments and are listed in Table 1. They are model eclogite compositions in the system SiO_2–Al_2O_3–MgO–FeO–CaO–Na_2O–CO_2, designed to crystallise garnet + omphacitic clinopyroxene + calcite-dolomite solid solution under high-pressure sub-solidus conditions. EC2 is more sodic than EC1, but contains other oxides in identical proportions to EC1. EC1 was used in the majority of the experiments, in which phase relations and carbonate partial melt compositions were determined from 2.5 to 5.5 GPa. The results of three experiments using EC2 are also reported. Yaxley (1999) reported an additional EC2 experiment, (C690) run at 3.5 GPa and 1,215 °C.

Table 1 Nominal model carbonated eclogite compositions used in the high pressure experiments. Mg# = 100*Mg/[Mg + $\sum$Fe] (molar proportions)

	EC1	EC2
SiO_2	30.11	29.16
Al_2O_3	11.74	11.37
FeO	10.05	9.73
MgO	12.44	12.05
CaO	19.41	18.80
Na_2O	0.87	4.00
CO_2	15.38	14.89
CaO/MgO	1.56	1.56
Mg#	68.82	69.82

EC1 and EC2 were prepared as mixtures of oxides of Si and Al, and carbonates of Mg and Na, ground to fine-grained homogenous powders under AR grade acetone. These mixtures were dehydrated and decarbonated by firing in air at 1,000 °C. FeO was then added as synthetic fayalite and CaO and CO_2 as analytical grade $CaCO_3$. These components were also blended under acetone with the fired powders, and the final mixtures were dried at 120 °C. Fifty-milligram samples of these materials were then run in large capacity assemblies in a piston-cylinder press at sub-solidus conditions of 3.5 GPa and 1,150 °C for 48 h, producing fine grained assemblages containing garnet, clinopyroxene and calcite–dolomite solid solution ($[\text{cc-dol}]_{ss}$). These materials were recovered at the end of the runs and ground back into the corresponding original mixtures to provide seeds to assist in nucleation of phases in subsequent experiments (Yaxley 1999).

High-pressure experimental techniques

Runs at 2.5, 3.0 and 3.5 GPa were performed using conventional 1.27 cm diameter piston-cylinder apparatuses at the Research School of Earth Sciences, Australian National University (ANU) and procedures are described elsewhere (Yaxley 1999). Experiments at 4.0, 4.3, 5.0 and 5.5 GPa were conducted using the belt apparatus at the Universität Frankfurt, following procedures of Brey et al. (1990). Run numbers for these experiments are prefixed with KW in Table 2. Pressures and temperatures for both piston-cylinder and belt apparatus runs are accurate to ±0.1 GPa and ±10 °C, respectively.

In all runs, sample materials were encapsulated in graphite inner capsules, which were sealed in welded Pt outer capsules. Experimental oxygen fugacity (fO_2) was therefore most likely at or below the CCO buffer. In some runs containing diopside and dolomitic carbonate and the additional phase coesite, fO_2 was probably buffered by the reaction dolomite + 2coesite = diopside + 2C + $2O_2$ (Luth 1993) to values below CCO at high pressure (Luth 1993). Run times varied from 51 to 356 h. Details of experimental runs and the assemblages produced are presented in Table 2.

Analytical techniques

Run products were examined using a JEOL 6400 scanning electron microscope at the Electron Microscopy Unit, ANU. Crystalline phases and quenched liquids were analysed by energy dispersive electron-probe microanalysis using an accelerating voltage of 15 kV, a beam current of 1 nA and a LINK detector. Because of the tendency for carbonate liquids present in experimental runs to quench to heterogeneous assemblages of metastable phases, reported melts compositions (Table 3) are averages of multiple broad beam scans across large areas of pooled quenched melt. In some runs, this was facilitated by a tendency for the liquid to partially segregate to one end of the capsule, forming larger pools. In some other runs accurate melt compositions could not be determined. Crystalline phases were analysed with a focussed electron beam with a 1 μm diameter, and reported phase compositions (Tables 4, 5, 6) are averages of multiple analyses. Detection limits for minor element oxides such as Na_2O in garnet or SiO_2 in carbonate were typically 0.10 wt%.

We were unable to determine accurate phase or quenched liquid compositions from run C694 due to its very fine grain size, although an assemblage of garnet, clinopyroxene, carbonate and quenched liquid was clearly present. Similarly, in run KW1262EC2, we could not obtain a reasonable estimate of the quenched liquid composition.

Table 2 Details of experimental runs, including P, T, run duration, assemblages and mass proportions of each phase present. *ga* Garnet; *cpx* clinopyroxene; *co* coesite; *[cc-dol]$_{ss}$* calcite–dolomite solid solution; *cb_{liq}* quenched carbonate liquid. Proportions of phases and liquid present in each run are in wt% and were estimated from least squares mass balance calculations using nominal bulk compositions, and average phase and melt compositions determined from electron-probe microanalysis. CO_2 contents of carbonates were calculated from measured oxide abundances assuming CO_2 was present as $CaCO_3$, $MgCO_3$, $FeCO_3$ and, in the case of carbonate liquid, Na_2CO_3. Note that phase compositions and, therefore, proportions could not be determined from run C694 due to its very fine grain size, nor from KW1262EC2 as a melt composition was unobtainable

Run no.	Duration (h)	P (GPa)	T(°C)	Assemblage	ga	cpx	co	[cc-dol]$_{ss}$	cb_{liq}	Σr^2
EC1 runs										
Belt apparatus (Frankfurt)										
KW223	200	5.5	1,200	ga + cpx + co + [cc-dol]$_{ss}$	47.0	14.5	2.8	35.7	0.0	0.3
KW205	168	5	1,100	ga + cpx + co + [cc-dol]$_{ss}$	44.8	20.7	0.1	34.4	0.0	0.2
KW209	168	5	1,200	ga + cpx + co + [cc-dol]$_{ss}$	45.4	19.9	0.3	34.3	0.0	1.2
KW206	168	5	1,300	ga + cpx + co + [cc-dol]$_{ss}$	49.3	14.6	1.9	34.2	0.0	0.1
KW221	120	5	1,340	ga + cpx + co + [cc-dol]$_{ss}$ + cb_{liq}	46.4	17.2	0.0	9.4	26.9	0.1
KW211	74	5	1,400	ga + cpx + cb_{liq}	45.7	19.4	0.0	0.0	34.9	0.4
KW214	188	4.3	1,100	ga + cpx + co + [cc-dol]$_{ss}$	45.8	19.8	0.6	33.9	0.0	0.1
KW215	192	4.3	1,200	ga + cpx + co + [cc-dol]$_{ss}$	45.9	19.5	0.6	34.0	0.0	0.1
KW226	220	4.3	1,240	ga + cpx + [cc-dol]$_{ss}$	48.6	19.0	0.0	32.4	0.0	1.8
KW216	141	4.3	1,300	ga + cpx + co + [cc-dol]$_{ss}$ + cb_{liq}	47.0	16.7	0.0	7.9	28.4	0.2
KW1259	168	4	1,100	ga + cpx + [cc-dol]$_{ss}$	44.6	21.8	0.0	33.6	0.0	0.4
KW1263	168	4	1,150	ga + cpx + [cc-dol]$_{ss}$	44.1	22.8	0.0	33.1	0.0	1.4
KW1261	168	4	1,200	ga + cpx + [cc-dol]$_{ss}$	46.8	19.5	0.0	33.8	0.0	0.9
Piston cylinder (Canberra)										
C602	168	3.5	1,180	ga + cpx + [cc-dol]$_{ss}$	51.5	16.2	0.0	32.3	0.0	3.6
C649	70	3.5	1,215	ga + cpx + [cc-dol]$_{ss}$	53.7	14.8	0.0	31.4	0.0	8.2
C694	165	3.5	1,250	ga + cpx + [cc-dol]$_{ss}$ + cb_{liq}	nd	nd	nd	nd	nd	nd
C647	70	3.3	1,275	ga + cpx + [cc-dol]$_{ss}$ + cb_{liq}	47.1	18.0	0.0	1.3	33.6	0.7
C658	116	3.5	1,300	ga + cpx + cb_{liq}	47.6	16.1	0.0	0.0	36.3	0.4
C688	51	3.5	1,400	ga + cb_{liq}	57.9	0.0	0.0	0.0	42.1	9.1
C681	240	3	1,100	ga + cpx + [cc-dol]$_{ss}$	48.5	18.7	0.0	32.8	0.0	1.8
C661	170	3	1,180	ga + cpx + [cc-dol]$_{ss}$ + cb_{liq}	45.7	19.3	0.0	8.4	26.7	0.3
C643	215	3	1,250	ga + cpx + cb_{liq}	46.9	17.9	0.0	0.0	35.2	1.1
C1079	356	2.5	1,100	ga + cpx + [cc-dol]$_{ss}$	50.1	18.0	0.0	31.9	0.0	5.5
C1084	240	2.5	1,150	ga + cpx + [cc-dol]$_{ss}$ + cb_{liq}	43.7	22.7	0.0	0.4	33.2	0.7
EC2 runs										
Belt apparatus (Frankfurt)										
KW205EC2	168	5	1,100	ga + cpx + [cc-dol]$_{ss}$	45.0	20.6	0.0	34.5	0.0	11.1
KW1261EC2	168	4	1,200	ga + cpx + cb_{liq}	42.6	20.4	0.0	0.0	37.0	4.8
KW1262EC2	168	4	1,240	ga + cpx + cb_{liq}	n.d.	n.d.	n.d.	n.d.	n.d.	n.d.
Piston cylinder (Canberra)										
C690EC2	168	3.5	1,215	ga + cpx + cb_{liq}	45.9	21.6	0.0	0.0	32.5	2.5

Experimental results

Phase relations and phase compositions

Runs produced well-crystallised assemblages of garnet ± carbonate ± clinopyroxene ± coesite. Crystals of garnet, clinopyroxene and coesite were typically ≤ 20 μm in diameter and euhedral to subhedral in shape. Back scattered electron images of representative run products are presented in Fig. 1.

Garnets were essentially solid solutions of pyrope, grossular and almandine, although a minor presence of andradite cannot be ruled out. Garnet Mg# [100*Mg/(Mg + $\sum$Fe)] generally increased with increasing temperature (Table 5). At a given temperature, lower pressure garnets (2.5–3.5 GPa) generally had lower Ca and higher Mg contents than those crystallised at higher pressures (4.0–5.5 GPa). For example, garnet in 1,100 °C runs C1079 and C681 (2.5 and 3.0 GPa) had X_{Ca} of 19.5 and 18.6 (where X_{Ca} = 100*Ca/[Mg + Ca + Fe]), and X_{Mg} of 50.2 and 50.1, respectively. In 1,100 °C runs, KW214 and KW205 (4.3 and 5.0 GPa) garnets had X_{Ca} of 25.2 and 23.9, and X_{Mg} of 43.1 and 44.7 mol% pyrope, respectively.

Clinopyroxenes were dominantly solid solutions of diopside, jadeite and Tschermak's components (Table 6). Na_2O contents decreased systematically with increasing temperature at each pressure, particularly with increasing degrees of melting (Fig. 2) at temperatures above the solidus. For runs at similar temperatures, clinopyroxenes crystallised at higher pressures were usually richer in Na_2O, presumably due to higher jadeite contents (Fig. 2). Clinopyroxene Mg# was fairly constant in all runs, ranging from 77.0 (C1084) to 81.7 (KW214). Variation in molar Ca:Mg:Fe ratio was minor.

Table 3 Quenched liquid compositions from the experimental run products. Data are averages of n broad electron beam scans of pools of quenched liquid. Na# = $Na_2CO_3/[Na_2CO_3 + CaCO_3 + MgCO_3 + FeCO_3]$ Mg# = $100*Mg/[Mg + \sum Fe]$. X_{Ca}, X_{Mg} and X_{Fe} are the mole fractions of Ca, Mg and Fe respectively

	EC1										EC2	
	C1084	C643	C661	C688	C658	C647	KW216	KW211	KW221	KW206	C690	KW1261
P (GPa)	2.5	3	3	3.5	3.5	3.5	4.3	5	5	5	3.5	4
T (°C)	1,150	1,250	1,180	1,400	1,300	1,275	1,300	1,400	1,340	1,300	1,215	1,200
n	(5)	(5)	(6)	(10)	(5)	(6)	(5)	(5)	(10)	(2)	(10)	(3)
SiO_2	1.27	4.63	3.82	12.62	6.30	3.44	6.18	2.05	5.16	0.39	2.57	3.37
Al_2O_3	0.21	0.65	1.24	2.34	0.74	0.43	0.69	0.79	1.74	0.22	0.73	0.59
FeO	5.77	7.17	6.71	6.96	8.38	6.65	7.68	8.06	8.46	7.10	4.05	7.66
MgO	10.26	9.13	11.09	10.04	9.45	10.23	8.58	9.89	9.36	9.08	9.62	8.24
CaO	34.89	32.08	30.98	31.15	32.75	31.52	32.02	35.06	32.25	35.85	31.82	25.82
Na_2O	1.12	2.22	2.21	1.61	2.13	2.08	1.18	0.12	0.56	0.20	4.92	3.58
Total	53.53	55.88	56.05	64.72	59.75	54.34	56.33	55.96	57.53	52.83	53.71	49.26
Mg#	76.00	69.40	74.65	71.99	66.77	73.28	66.58	68.62	66.35	69.50	80.89	65.72
X_{Ca}	65.01	63.69	60.00	61.63	62.46	61.88	64.11	63.62	62.18	66.36	65.80	59.69
X_{Mg}	26.60	25.20	29.86	27.63	25.06	27.94	23.89	24.97	25.09	23.38	27.67	26.49
X_{Fe}	8.40	11.11	10.14	10.75	12.47	10.19	12.00	11.42	12.72	10.26	6.54	13.82
Na#	0.0186	0.0383	0.0373	0.0280	0.0354	0.0356	0.0209	0.0019	0.0096	0.0033	0.0843	0.0697

Table 4 Compositions of carbonate grains inferred to have been crystalline at run P–T conditions. Symbols as in Table 3

	EC1									
	C1084	C1079	C661	C681	C647	C649	C602	KW1261	KW1263	KW1259
P (GPa)	2.5	2.5	3	3	3.5	3.5	3.5	4	4	4
T (°C)	1,150	1,100	1,180	1,100	1,275	1,215	1,180	1,200	1,150	1,100
n	(10)	(15)	(7)	(10)	(10)	(6)	(5)	(10)	(8)	(9)
SiO_2	0.26	0.67	0.52	0.25	0.15	0.62	0.70	0.91	0.20	0.30
Al_2O_3	0.10	0.24	0.25	0.14	0.15	0.17	0.26	0.18	0.10	0.15
FeO	2.68	3.49	2.79	4.53	1.89	3.34	4.15	5.46	5.96	5.94
MgO	6.03	7.05	5.49	8.48	4.62	5.77	7.32	8.65	10.92	10.82
CaO	44.80	40.83	44.39	39.64	47.76	41.56	43.78	37.36	34.07	34.71
Na_2O	0.13	0.08	0.09	0.06	0.00	0.00	0.02	0.04	0.01	0.01
Total	53.99	52.36	53.52	53.10	54.57	51.46	56.23	52.61	51.25	51.93
Mg#	80.00	78.26	77.82	76.94	81.31	75.52	75.86	73.85	76.55	76.45
X_{Ca}	81.05	76.53	81.91	72.11	85.80	79.63	76.54	69.63	63.20	63.80
X_{Mg}	15.16	18.37	14.08	21.46	11.55	15.38	17.80	22.43	28.17	27.67
X_{Fe}	3.79	5.10	4.01	6.43	2.65	4.99	5.66	7.94	8.63	8.52
										EC2
	KW216	KW226	KW215	KW214	KW221	KW206	KW209	KW205	KW223	KW205
P (GPa)	4.3	4.3	4.3	4.3	5	5	5	5	5.5	5
T (°C)	1,300	1,240	1,200	1,100	1,340	1,300	1,200	1,100	1,200	1,100
n	(5)	(10)	(10)	(10)	(4)	(8)	(3)	(9)	(12)	16
SiO_2	1.15	0.48	0.41	0.49	0.25	0.26	0.56	1.17	0.62	2.01
Al_2O_3	0.37	0.15	0.17	0.19	0.16	0.16	0.35	0.59	0.29	0.77
FeO	6.67	5.53	6.23	6.29	6.66	6.16	5.56	5.73	6.93	5.73
MgO	9.27	10.96	12.37	12.89	9.86	10.11	12.97	13.36	13.76	13.76
CaO	36.43	37.04	34.52	33.20	36.18	35.81	33.59	32.67	30.75	33.78
Na_2O	0.22	0.19	0.15	0.14	0.22	0.22	0.07	0.22	0.16	0.12
Total	54.12	54.34	53.86	53.19	53.33	52.70	53.10	53.73	52.51	56.17
Mg#	71.25	77.94	77.97	78.51	72.52	74.52	80.61	80.61	77.95	80.58
X_{Ca}	66.80	65.45	61.00	59.25	65.68	65.50	60.02	58.63	55.60	59.07
X_{Mg}	23.65	26.93	30.41	31.99	24.89	25.71	32.23	33.35	34.61	33.08
X_{Fe}	9.55	7.62	8.59	8.76	9.43	8.79	7.75	8.02	9.79	7.85

In some runs at P > 4.0 GPa a minor phase consisting almost entirely of SiO_2 with minor Al_2O_3 crystallised as rounded grains less than 20 μm across (Fig. 1A). This is inferred to be coesite as the run pressures are considerably higher than the lower pressure limit for coesite stability in the SiO_2 system (Bose and Ganguly 1995). Coesite is possibly formed as a result of the reaction diopside + $2CO_2$ = dolomite + 2coesite, which was determined in P–T space for pure phases by Luth (1995) and is plotted in Fig. 3.

Carbonate textures were complex and variable. In higher temperature runs across the investigated pressure range (e.g. KW211, C658, C688), carbonate exhibited quench-related textures (Fig. 1B–D) consisting mainly of heterogeneous assemblages of crystals, including dolomite and an unidentified Fe-rich silicate phase. This

Table 5 Garnet compositions from the experimental run products. Data are averages of n analyses of individual grains. Symbols as in Table 3

EC1														
	C1084	C1079	C643	C661	C681	C688	C658	C647	C649	C602	KW1261	KW1263	KW1259	KW216
P (GPa)	2.5	2.5	3	3	3	3.5	3.5	3.5	3.5	3.5	4	4	4	4.3
T (°C)	1,150	1,100	1,250	1,180	1,100	1,400	1,300	1,275	1,215	1,180	1,200	1,150	1,100	1,300
n	(8)	(10)	(11)	(9)	(10)	(10)	(6)	(12)	(7)	(4)	(10)	(9)	(7)	(7)
SiO_2	40.58	40.58	40.73	41.09	41.14	41.73	40.84	40.97	40.84	41.00	40.97	40.94	40.60	40.94
Al_2O_3	23.04	22.72	22.66	22.70	22.29	22.72	22.46	22.55	22.33	22.26	22.95	22.72	22.67	22.32
FeO	14.97	15.00	13.04	14.33	15.47	10.90	12.93	13.44	14.96	15.28	14.94	15.34	15.78	13.99
MgO	14.15	13.94	13.33	14.10	13.89	14.18	13.57	14.29	13.88	14.58	13.90	13.34	12.62	14.03
CaO	7.13	7.54	10.23	7.72	7.15	10.41	10.20	8.75	7.99	6.82	7.19	7.61	8.28	8.55
Na_2O	0.14	0.21	0.01	0.07	0.06	0.07	0.00	0.00	0.00	0.05	0.05	0.05	0.06	0.17
Mg#	62.74	62.35	64.56	63.68	61.54	69.87	65.16	65.46	62.30	62.96	62.38	60.79	58.77	64.12
X_{Ca}	18.53	19.52	26.25	20.05	18.56	26.94	26.03	22.38	20.51	17.48	18.84	19.95	21.70	21.94
X_{Mg}	51.12	50.18	47.61	50.92	50.11	51.05	48.20	50.81	49.52	51.96	50.62	48.66	46.02	50.05
X_{Fe}	30.35	30.30	26.14	29.04	31.32	22.01	25.77	26.81	29.97	30.56	30.53	31.39	32.28	28.01

										EC2			
	KW226	KW215	KW214	KW211	KW221	KW206	KW209	KW205	KW223	C690	KW1261	KW1262	KW205
P (GPa)	4.3	4.3	4.3	5	5	5	5	5	5.5	3.5	4	4	5
T (°C)	1,240	1,200	1,100	1,400	1,340	1,300	1,200	1,100	1,200	1,215	1,200	1,240	1,100
n	(11)	(10)	(10)	(20)	(9)	(10)	(16)	(9)	(9)	(10)	(10)	(6)	(21)
SiO_2	40.82	40.77	40.57	41.18	41.50	41.01	41.17	40.72	40.69	39.86	40.80	40.96	40.36
Al_2O_3	21.91	22.06	22.15	22.65	21.89	22.13	22.34	22.08	21.93	23.14	22.80	22.94	22.27
FeO	14.66	15.38	15.59	13.09	13.45	14.24	14.75	15.42	14.95	13.05	13.66	13.22	13.74
MgO	13.69	12.75	11.87	14.53	14.45	13.85	13.61	12.35	11.77	12.12	13.26	13.70	12.55
CaO	8.65	8.86	9.65	8.49	8.51	8.48	8.04	9.20	10.47	11.71	9.40	9.16	10.80
Na_2O	0.28	0.18	0.17	0.07	0.21	0.28	0.09	0.23	0.19	0.12	0.08	0.03	0.28
Mg#	62.47	59.64	57.57	66.41	65.70	63.42	62.17	58.80	58.38	62.34	63.35	64.87	61.96
X_{Ca}	22.11	22.95	25.18	21.81	21.75	21.82	20.90	23.94	27.18	30.22	24.41	23.77	27.70
X_{Mg}	48.66	45.95	43.07	51.93	51.41	49.58	49.18	44.72	42.52	43.50	47.89	49.45	44.79
X_{Fe}	29.24	31.10	31.75	26.26	26.84	28.60	29.92	31.34	30.31	26.28	27.70	26.78	27.50

Table 6 Clinopyroxene compositions from the experimental run products. Symbols as in Table 3

EC1														
	C1084	C1079	C643	C661	C681	C688	C658	C647	C649	C602	KW1261	KW1263	KW1259	KW216
P (GPa)	2.5	2.5	3	3	3	3.5	3.5	3.5	3.5	3.5	4	4	4	4.3
T (°C)	1,150	1,100	1,250	1,180	1,100	1,400	1,300	1,275	1,215	1,180	1,200	1,150	1,100	1,300
n	(9)	(15)	(9)	(9)	(9)		(5)	(8)	(5)	(7)	(10)	(5)	(5)	(3)
SiO_2	51.17	51.52	50.54	52.33	53.10	n.a.	51.75	51.70	52.00	52.30	54.34	54.43	54.48	53.64
Al_2O_3	6.50	6.74	7.06	5.25	6.42	n.a.	5.66	5.52	4.60	4.51	6.44	6.88	7.24	5.71
FeO	7.58	7.19	6.68	7.13	6.86	n.a.	6.56	6.48	7.18	7.07	5.96	5.41	5.32	5.98
MgO	14.23	13.79	14.43	15.05	13.74	n.a.	14.76	15.10	15.48	14.89	13.28	12.81	12.42	13.94
CaO	19.21	18.92	20.86	19.11	17.93	n.a.	20.92	20.83	19.94	19.69	17.39	17.48	17.43	18.81
Na_2O	1.31	1.83	0.42	1.14	1.95	n.a.	0.35	0.38	0.80	1.53	2.59	2.99	3.12	1.92
Mg#	76.98	77.35	79.37	79.00	78.10		80.04	80.59	79.34	78.98	79.87	80.85	80.60	80.59
X_{Ca}	42.76	43.29	45.21	41.90	42.29		44.92	44.43	42.35	42.87	42.92	44.23	44.86	43.88
X_{Mg}	44.06	43.87	43.49	45.90	45.07		44.09	44.78	45.74	45.12	45.59	45.09	44.45	45.23
X_{Fe}	13.18	12.85	11.30	12.20	12.64		10.99	10.79	11.91	12.01	11.49	10.68	10.70	10.89

										EC2			
	KW226	KW215	KW214	KW211	KW221	KW206	KW209	KW205	KW223	C690	KW1261	KW1262	KW205
P (GPa)	4.3	4.3	4.3	5	5	5	5	5	5.5	3.5	4	4	5
T (°C)	1,240	1,200	1,100	1,400	1,340	1,300	1,200	1,100	1,200	1,215	1,200	1,240	1,100
n	(10)	(10)	(10)	(25)	(5)	(5)	(16)	(5)	(5)	(10)	(7)	(6)	(24)
SiO_2	50.53	54.61	54.68	54.25	54.46	54.43	54.77	54.75	54.85	50.02	54.25	53.51	54.21
Al_2O_3	6.68	7.23	7.22	6.19	5.92	6.11	6.48	7.65	7.28	9.44	7.08	8.35	8.83
FeO	6.36	5.23	4.78	5.71	5.46	5.61	5.67	4.80	4.77	5.88	5.16	5.14	4.30
MgO	13.41	12.07	11.97	13.71	13.60	13.18	12.96	11.62	11.86	12.70	12.82	12.49	11.32
CaO	20.44	17.54	17.88	17.87	18.14	17.74	17.18	16.91	17.55	20.21	17.68	17.62	16.41
Na_2O	2.59	3.32	3.48	2.27	2.42	2.94	2.94	4.27	3.69	1.75	3.00	2.89	4.94
Mg#	78.98	80.46	81.69	81.05	81.61	80.72	80.30	81.16	81.58	79.38	81.56	81.24	82.42
X_{Ca}	46.40	45.66	46.74	43.15	43.90	43.87	43.35	45.93	46.46	47.59	44.71	45.17	46.21
X_{Mg}	42.33	43.72	43.51	46.08	45.79	45.31	45.49	43.89	43.68	41.60	45.09	44.55	44.33
X_{Fe}	11.27	10.62	9.75	10.77	10.31	10.82	11.16	10.18	9.86	10.81	10.19	10.29	9.46

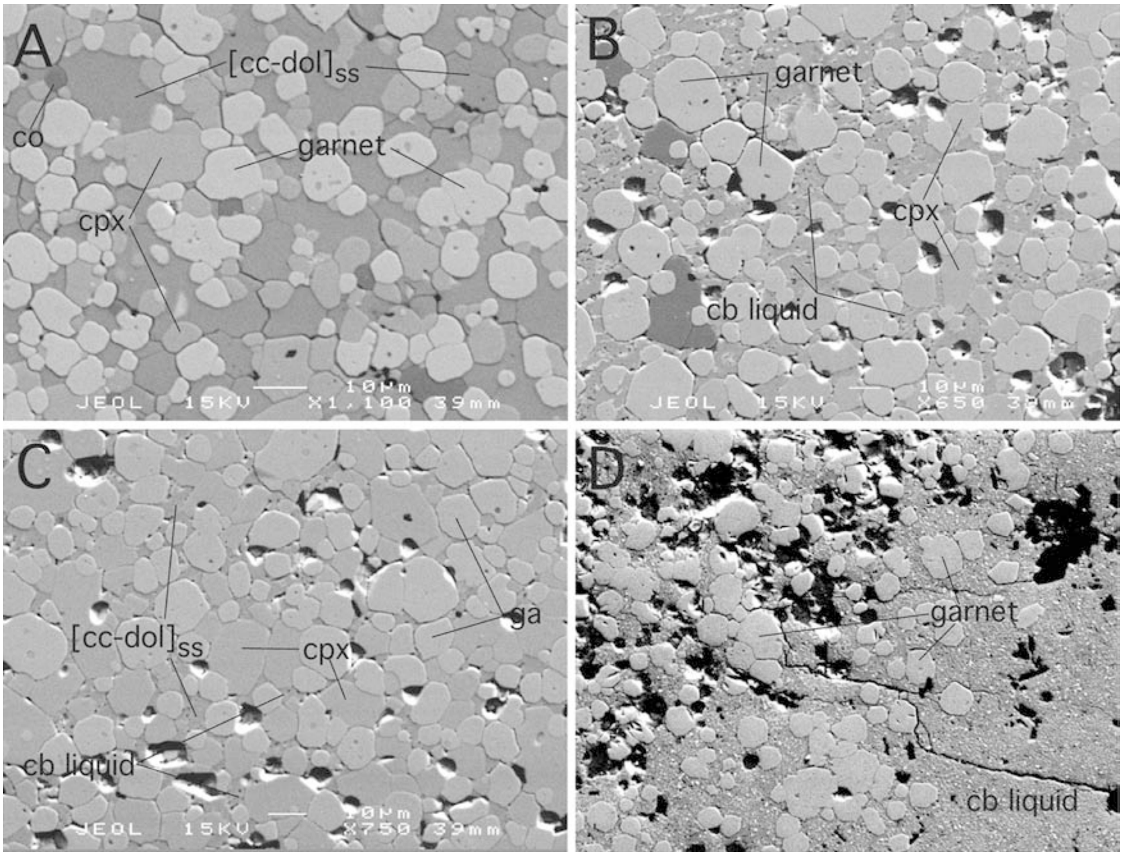

Fig. 1A–D Backscattered electron images of high-pressure products of experiments using EC1. *Scale bars* represent 10 μm. **A** Run KW223 (5.5 GPa and 1,200 °C), showing subsolidus assemblage of garnet + clinopyroxene (cpx) + calcite–dolomite solid solution ([cc-dol]$_{ss}$) and minor coesite (co). **B**, **C** Run KW221 (5 GPa and 1,340 °C) showing partially molten assemblages of garnet + cpx + [cc-dol]$_{ss}$ + quenched carbonatitic liquid (cb liquid). Image **B** was taken near the top of the capsule and contains a higher proportion of quenched melt than **C**, which was taken from the central portion of the capsule. This indicates that melt partially segregated during the run forming larger pools near the top of the capsule. Note the clear quench related textures in **B** and small carbonate grains in **C** interpreted to have been crystalline at run conditions on compositional grounds. See the text for further explanation. **D** Run C688 (3.5 GPa and 1,400 °C) showing large degree (42%; Table 2) of quenched partial melt and garnet residue. Melt has clearly segregated to the part of the capsule depicted in *bottom right hand corner* of the image

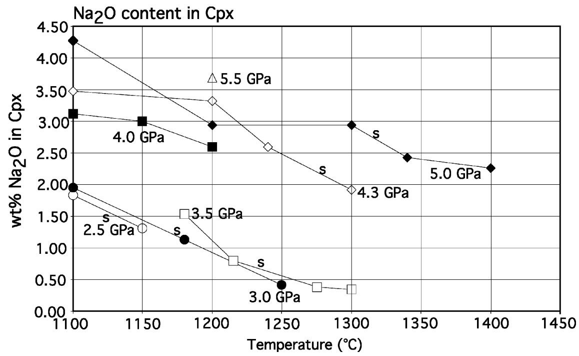

Fig. 2 Na_2O content in wt% in experimentally crystallised clinopyroxene grains. Run pressures are indicated, and the small '*s*' near the data for runs at each pressure indicates the approximate solidus temperature at that pressure

assemblage is inferred to have been molten at run conditions. In runs with relatively high melt fractions, the liquid exhibited a clear tendency to partially segregate and quench in pools at the upper end of the capsule (Fig. 1D), or as pools within the crystalline residual assemblage. Carbonate liquid compositions presented in Table 3 were determined by averaging multiple broad electron beam analyses of segregated or pooled areas of quenched material.

Quenched liquid compositions are presented in Table 3. They are broadly calcio-dolomitic in composition, containing 59.7–66.4 mol% $CaCO_3$, 23.4–29.9 mol% $MgCO_3$ and 6.5–13.8 mol% $FeCO_3$. With the exception of run KW206 (EC1 at 5 GPa, 1,300 °C), the liquid compositions were always lower in $CaCO_3$ than coexisting carbonate that was crystalline at run P-T conditions (see below), although the differences decreased with increasing pressure (Fig. 4). Liquid SiO_2 contents increased with temperature at a given pressure. For example, in EC1 runs conducted at 3.5 GPa, SiO_2 content varied from 3.4 wt% at 1,275 °C, 6.3 wt% at 1,300 °C to 12.6 wt% at 1,400 °C. Runs at 3.0 and 3.5 GPa demonstrate that liquid Na_2O content was fairly constant at ≈2.1 wt% for liquids in equilibrium with clinopyroxene, but decreased above clinopyroxene-out. For example, quenched liquid in a run at 3.5 GPa and 1,400 °C contained 1.6 wt% Na_2O. Melts formed in

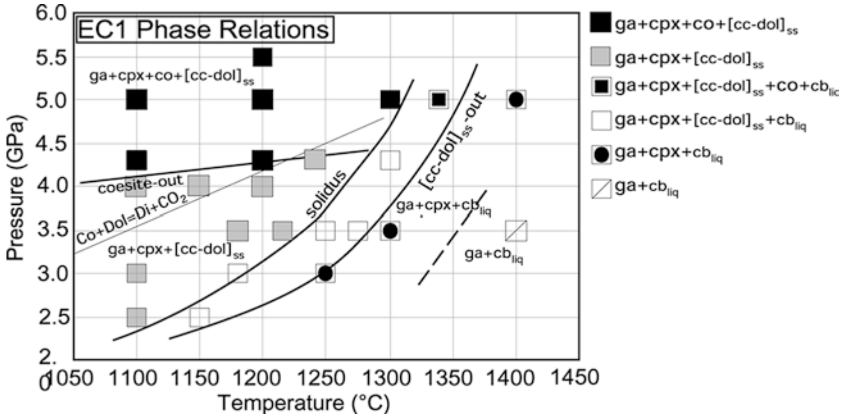

Fig. 3 Phase relations in PT space for EC1, indicating estimated solidus position, assemblages present in experiments and various phase-out boundaries. The reaction 2 coesite (Co) + dolomite (Dol) = diopside (Di) + $2CO_2$ was determined for pure phases by Luth (1995). *Abbreviations* as in Table 2

EC2 runs were similar to those formed in EC1 runs, but were notably higher in Na_2O content, consistent with the higher bulk Na_2O content of EC2 compared with EC1. For example, liquid in run C690EC2 contained 4.9 wt% Na_2O, the highest of any melt in these experiments.

The accuracy of the measured liquid compositions was tested by performing least squares mass balance calculations using the measured phase and liquid compositions, and the nominal bulk compositions. All runs except C694 and KW1262EC2 gave satisfactory mass balances, indicating that for most above solidus experiments, the measured melt compositions are reasonable estimates of the equilibrium partial melt compositions (Table 2).

In lower temperature runs, quench textures were absent. Carbonate crystallised as compositionally homogenous grains interstitial to silicate phases (Fig. 1A). This type of carbonate is inferred to have been crystalline at run pressure–temperature conditions. Reported compositions (Table 4) are averages of multiple analyses using a focused 1 μm diameter electron beam. Compositions are calcite–dolomite solid solutions and exhibited minimal compositional variation on an intra-run basis, consistent with a close approach to equilibrium in most runs. However, average compositions of carbonate crystallised in different runs exhibited systematic variations with pressure and temperature, tending towards higher calcite and lower dolomite as temperature increased at a given pressure, and as pressure decreased at constant temperature (Fig. 4). This effect is less significant in higher pressure runs. Carbonate Mg# varied from 73.9 to 80.6 in subsolidus runs.

Some runs at intermediate temperatures contained both crystalline and quenched carbonate. In these cases, carbonate crystals formed from carbonate liquid on quenching were difficult to distinguish from carbonate grains that were crystalline at run PT conditions on textural grounds alone. Instead, carbonate compositions were used; for example, primary crystalline carbonate contained minimal or no detectable Na_2O or SiO_2, and had Mg# distinctly higher than coexisting quenched carbonate and also the silicates. They were similar to carbonates from lower temperature runs with no apparent quench textures (Fig. 4). For example, in run KW221 (5 GPa and 1,340 °C), carbonate which is interpreted as crystalline at run P–T, had Mg# = 72.5, whereas quenched carbonate liquid had Mg# = 66.4. X_{Ca} was broadly similar for both types of carbonate in this run, but the quenched liquid had higher SiO_2 and Na_2O contents (Tables 3 and 4).

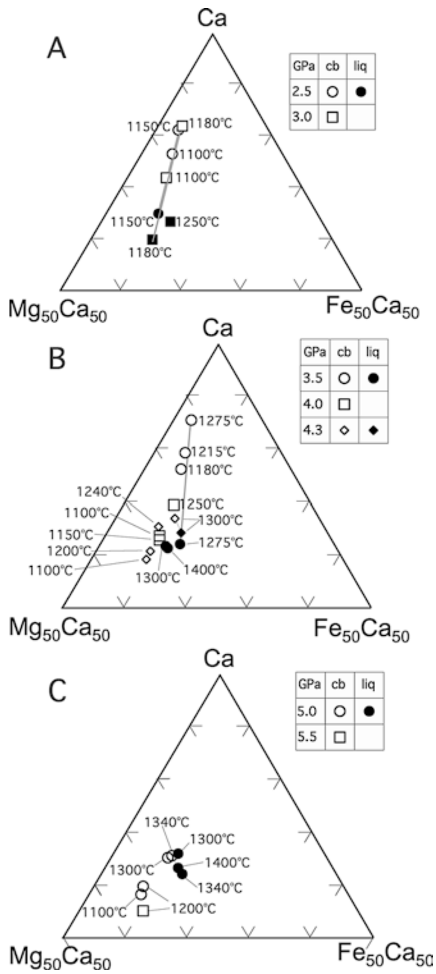

Fig. 4 Compositions in $CaCO_3$–$MgCO_3$–$FeCO_3$ space of carbonate inferred to have been crystalline (*open symbols*) and carbonate inferred to have quenched from carbonatitic liquids present in the experiments (*filled symbols*) at run PT conditions. Run temperatures indicated beside *symbols*. Grey tie lines join coexisting solid and quenched carbonate. See text for further explanation

$$\underset{\text{dolomite}}{3CaMg(CO_3)_2} + \underset{\text{grossular}}{Ca_3Al_2Si_3O_{12}} = \underset{\text{calcite}}{6CaCO_3} + \underset{\text{pyrope}}{Mg_3Al_2Si_3O_{12}} \quad (1)$$

Based on the above interpretation of carbonate compositions and textures, phase relations for EC1 are summarised in Fig. 3. A high-pressure, subsolidus field contains the assemblage garnet + clinopyroxene + $[\text{cc-dol}]_{ss}$ + coesite, where $[\text{cc-dol}]_{ss}$ is inferred to have been crystalline at run conditions. Coesite-out extends from about 1,100 °C at 4.1 GPa to intersect the solidus at 4.5 GPa and 1,290 °C. At lower pressure the assemblage consists of garnet + clinopyroxene + $[\text{cc-dol}]_{ss}$. The solidus varies from ≈1,125 °C at 2.5 GPa to ≈1,310 °C at 5 GPa. The phase boundary $[\text{cc-dol}]_{ss}$-out lies about 50 °C above the solidus over the investigated pressure range. A phase field therefore exists between the solidus and $[\text{cc-dol}]_{ss}$-out in which garnet + clinopyroxene + $[\text{cc-dol}]_{ss}$ ± coesite coexist with carbonate liquid. At temperatures above $[\text{cc-dol}]_{ss}$-out, garnet + clinopyroxene coexist with carbonate liquid. Clinopyroxene-out was not located precisely, but lies between 1,300 and 1,400 °C at 3.5 GPa. At temperatures above clinopyroxene-out the assemblage is garnet + carbonate liquid.

The EC2 runs KW1262EC2 and C690EC2 illustrate the strong effect of Na_2O in fluxing melting in carbonate systems. In both cases, experiments run at identical P–T conditions with EC1 crystallised melt-free assemblages, compared with the high proportion of melt (> 30 wt%) present in equilibrium with garnet + clinopyroxene in the EC2 runs.

Discussion

Approach to equilibrium

A reasonable approach to equilibrium in the runs is indicated by homogeneity of analyses of multiple crystals of each phase within a particular experimental assemblage. Also, carbonate in the EC1 and EC2 starting mixes was in the form of pure $CaCO_3$ (calcite) whereas experimental run products contain calcite–dolomite solid solutions, indicating reaction and an approach to equilibrium during the runs.

The garnet–clinopyroxene Fe–Mg exchange geothermometer of Ellis and Green (1979) was applied to coexisting garnet and clinopyroxene. In all cases (except C1079), calculated temperatures were within 100 °C of nominal run temperatures, and many were within 50 °C. This result is indicative of a reasonable approach to equilibration for interphase Fe–Mg exchange.

Ca–Mg partitioning between garnet and carbonate

Phase compositions are indicative of exchange reactions between garnet and carbonate:

such that high pressure and low temperature favour a higher mole fraction of dolomite in carbonate and a higher grossular content in garnet.

A plot of $\ln K_d$ vs $10^4/T$ (K) [where $K_d = (Ca/Mg)_{ga}/(Ca/Mg)_{cb}$] (Fig. 5) reveals a systematic pressure and temperature dependence of this exchange reaction. At constant pressure $\ln K_d$ is linearly correlated with inverse absolute temperature, and increasing pressure at constant temperature systematically increases $\ln K_d$. Runs conducted at 4.3 GPa plot at $\ln K_d$ values slightly higher than expected when compared with the remainder of the dataset, although the linear trend of increasing $\ln K_d$ with decreasing temperature is evident. We have no explanation for this apparent discrepancy at this stage.

Therefore, this exchange reaction has potential as a geobarometer for garnet + carbonate-bearing assemblages in the investigated P–T range, where carbonates are calcite–dolomite solid solutions and where temperature can be independently determined (e.g. through garnet–clinopyroxene Fe–Mg thermometry) although further experimentation (including reversals) are necessary for a rigorous calibration.

However, as a preliminary barometer, we have performed a fit of $RT\ln K_d$ as a linear function of P and T, according to the general equation:

$$\Delta G = \Delta H - \Delta S + P\Delta V + RT\ln K_d = 0$$

We have excluded the apparently anomalous 4.3 GPa data from this exercise. This produced the following equation, which can be used as an approximate geobarometer in the calibrated P–T range.

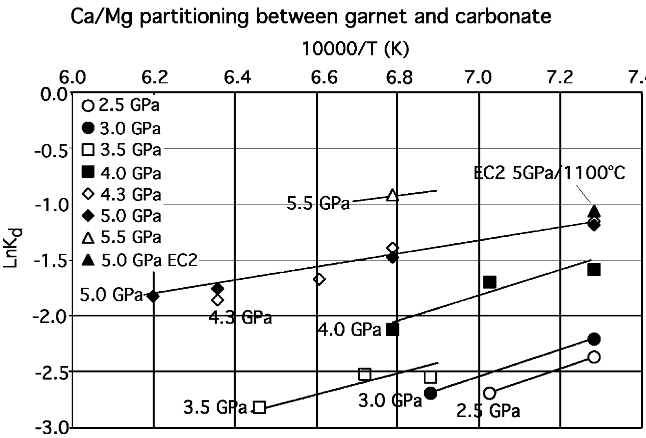

Fig. 5 Plot of $10^4/T$ (in Kelvin) vs $\ln K_d$ (where $K_d = [Ca/Mg]_{ga}/[Ca/Mg]_{cb}$), showing the pressure–temperature dependence of the garnet–carbonate exchange Reaction (1). Pressures are indicated. *Lines drawn through data points* at each pressure are visual estimates of line of best-fit, and have not been rigorously fitted. See text for further explanation

$$P(GPa) = 1.2978 \times 10^{-4} RT \ln K_d + 8.6297 \times 10^{-3} T - 5.4596 (T \text{ in Kelvin}, R = 8.31 JK^{-1} mol^{-1})$$

This equation reproduces the experimental pressures with a maximum discrepancy of 0.4 GPa, but is usually within 0.2 GPa. The model does not account for Ca–Mg non-ideality in garnet or carbonate: more rigorous refinement of the barometer will be the subject of future experimental investigations.

Hermann et al. (2001) reported evidence from natural rocks of the existence of exchange Reaction (1). Zoned garnets from dolomitic metacarbonates from the diamondiferous Kokchetav Massif had narrow rims exhibiting decreased Ca and increased Mg contents compared with large unzoned cores. This was interpreted as reflecting the occurrence of Reaction (1) between garnet and coexisting carbonate during decompression. Hermann et al. (2001) estimated a peak metamorphic temperature range of 950–1,000 °C based on garnet–clinopyroxene thermometry, and constrained the peak pressure to above the graphite–diamond transition (P > 4 GPa) and below the reaction aragonite + magnesite = dolomite (P < 6 GPa) (Luth 2001). Our preliminary calibration of the Ca–Mg partitioning between garnet and calcite–dolomite solid solution (Hermann, unpublished data) yielded a pressure of 5.2 GPa, in agreement with Hermann's estimate.

Carbonate-bearing eclogite melting relations

The garnet–carbonate exchange reactions [Reactions (1) and Fe-bearing equivalent] are important because the formation of calcite–dolomite solid solutions in high pressure garnet + carbonate assemblages controls melting behaviour of carbonate-bearing eclogite. This is because of the presence of a melting minimum on the $CaCO_3$–$MgCO_3$ join (Irving and Wyllie 1975; Byrnes and Wyllie 1981). At 2.7 GPa, the melting minimum on the join $CaCO_3$–$MgCO_3$ is at 1,300 °C (Irving and Wyllie 1975). Our estimate of the EC1 solidus temperature at 2.7 GPa is 1,150 °C, the difference most likely reflecting the effects of additional components such as FeO and Na_2O.

Figure 6 compares 2.7 GPa minimum melts on the $CaCO_3$–$MgCO_3$ join (Irving and Wyllie 1975) with partial melt compositions in equilibrium with garnet ± clinopyroxene ± $[\text{cc-dol}]_{ss}$ from the current experiments, experimental carbonatite liquids in equilibrium with amphibole- or phlogopite-bearing peridotite (Wallace and Green 1988; Thibault et al. 1992; Sweeney 1994) and those in equilibrium with Mg-calcite-bearing harzburgite or wehrlite (Dalton and Wood 1993). In the CaO–MgO–CO_2 system, minimum melts are broadly Mg-calcitic at 1.0 GPa (Byrnes and Wyllie 1981), but become more dolomitic at 2.7 GPa (Irving and Wyllie 1975). The liquids produced in the current experiments are very similar in Ca# to the 2.7-GPa minimum melt of Irving and Wyllie (1975), consistent with primary control on carbonate melt compositions in carbonated eclogite being the minimum melting relations on the calcite–magnesite join. They are, however, distinctly richer in $CaCO_3$, and lower in Mg# (Table 3), than dolomitic partial melts of carbonate-bearing amphibole or phlogopite lherzolite (Wallace and Green 1988; Thibault et al. 1992; Sweeney 1994). This is consistent with the absence of olivine or orthopyroxene in the eclogites produced here, and with the lower Mg# of EC1 compared with mantle peridotite.

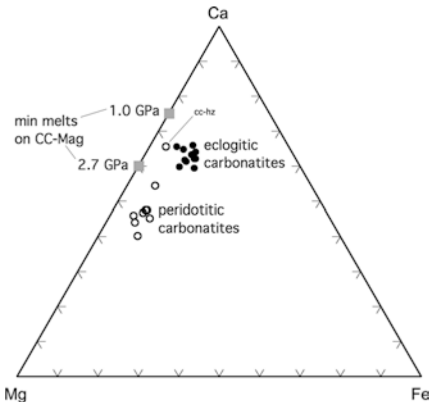

Fig. 6 Compositions in $CaCO_3$–$MgCO_3$–$FeCO_3$ space of carbonatites produced in equilibrium with eclogite in the current experiments (*filled circles*) compared with those produced experimentally in equilibrium with amphibole or phlogopite-bearing peridotitic assemblages. Peridotitic carbonatite compositions are from Thibault et al. (1992), Wallace and Green (1988) and Sweeney (1994). A more calcic liquid in equilibrium with calcite harzburgite produced by Dalton and Wood (1993) is indicated (cc-hz). Also shown are minimum melts on the join calcite–magnesite at 1 and 3 GPa (Irving and Wyllie 1975; Wyllie and Huang 1976; Byrnes and Wyllie 1981). With the exception of the compositions labelled *cc-hz*, eclogitic carbonatites are distinctly more calcic and have lower Mg/Fe than peridotitic carbonatites

Figure 7 is a plot of modal proportions of phases and melt using the results of the mass balance calculations for 5.0 and 3.5 GPa EC1 runs, summarised in Table 2. Similar results are obtained for experiments run at other pressures. These plots indicate that modal proportions of garnet and clinopyroxene are relatively unaffected by carbonate partial melting in the interval in which carbonatite liquid is in equilibrium with garnet, clinopyroxene and $[\text{cc-dol}]_{ss}$. Thus, the silicate phases are not contributing major quantities of components to the carbonatitic liquids present in the runs, and melting predominantly involves simple minimum melting of carbonate on the $CaCO_3$–$MgCO_3$ join. The run at 3.5 GPa and 1,400 °C (garnet + liquid) demonstrates that breakdown of clinopyroxene contributes components to the melt at higher degrees of melting, resulting in increased SiO_2 in the liquid.

However, the experiments also demonstrate that Na_2O has a strong effect on partial melting in carbonate systems. Solidus temperatures for the Na-rich

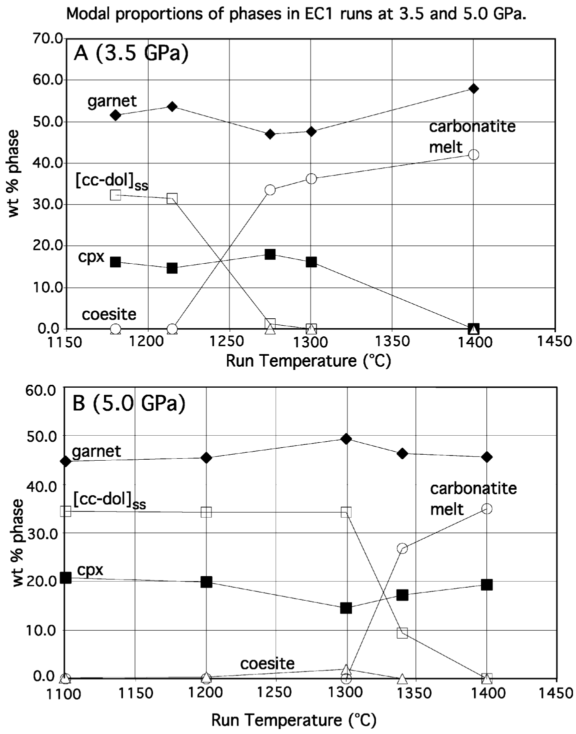

Fig. 7 Modal proportions of phases and liquid for runs at the representative pressures of **A** 3.5 and **B** 5.0 GPa. Modes are in wt% were determined from the bulk EC1 composition and phase and quenched liquid compositions measured by electron microprobe. See text for further information

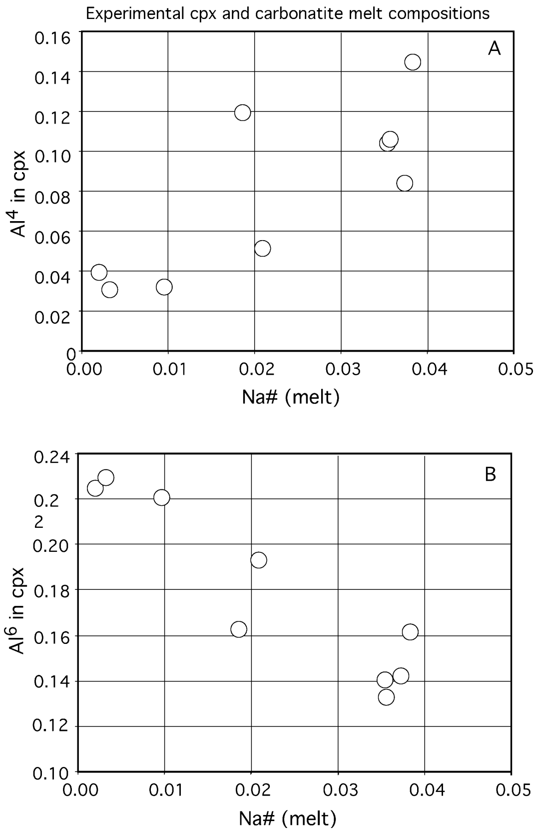

Fig. 8 Plots of **A** tetrahedral Al (Al^{IV}) and **B** octahedral Al (Al^{VI}) in clinopyroxene against Na# in coexisting liquid (where $Na\# = Na_2CO_3/[Na_2CO_3 + CaCO_3 + MgCO_3 + FeCO_3]$). Melts with higher Na# tend to have lower Al^{VI} and higher Al^{IV}, and vice versa. This is consistent with Na distribution between carbonatite melt and clinopyroxene being controlled by Reaction (2)

EC2 composition are clearly lower than those for the lower Na composition EC1. For example, the solidus of EC1 at 4.0 GPa is at about 1,260 °C, but lies between 1,100 and 1,200 °C for EC2. In subsolidus runs Na is mostly hosted in jadeite in clinopyroxene. Na distribution between jadeitic clinopyroxene and carbonatitic melt may be controlled by a reaction such as

$$\underset{[cpx]}{4NaAlSi_2O_6} + \underset{[carbonate]}{CaMg(CO_3)_2} = \underset{[melt]}{2Na_2CO_3} + \underset{[cpx]}{CaAl_2SiO_6} + \underset{[cpx]}{MgAl_2SiO_6} + \underset{[melt]}{6SiO_2} \quad (2)$$

If this is the case, then for a given bulk Na_2O content, carbonatite melts with high Na contents should coexist with clinopyroxene with high contents of Ca- and Mg-Tschermaks components and low jadeite components, compared with clinopyroxene in equilibrium with melts with lower Na contents. In Fig. 8, it is assumed that, for the clinopyroxenes crystallised in the current experiments, octahedral Al (Al^{VI}) is incorporated in jadeite and tetrahedral Al (Al^{IV}) is incorporated in Ca- or Mg-Tschermaks components. The fact that melts with higher Na# (where $Na\# = 100*Na_2CO_3/[Na_2CO_3 + CaCO_3 + MgCO_3 + FeCO_3]$) tend to have lower Al^{VI} and higher Al^{IV}, and vice versa (Fig. 8) is consistent with the above reaction controlling the distribution of Na zbetween clinopyroxene and carbonatite melt. This reaction allows prediction that (1) at higher pressures, where clinopyroxene is expected to be more jadeite-rich, carbonatite liquids should be lower in Na_2CO_3 compared with similar degrees of partial melting, and (2) at higher degrees of partial melting at given pressure, SiO_2 content of the carbonatite melt should increase. For example, several runs at various pressures have similar melt fractions (33–36%). With the exception of the run at 2.5 GPa (C1084), which contains melt with an unexpectedly low Na# of 1.86, Na# of melts decreases with increasing pressure from 3.8 at 3.0 GPa (C643) to 3.5 at 3.5 GPa (runs C658 and C647) to 0.9 at 5 GPa (run KW221). Secondly, in most cases, SiO_2 contents of melts increase with temperature at any pressure. Although our measured and unreversed melt compositions should only be considered estimates, their compositions are at least broadly consistent with control of their Na-contents by a reaction such as Reaction (2) above.

Formation of carbonatites from eclogite in the upper mantle.

Many altered oceanic basalts contain several wt% calcitic carbonate in veins and vugs, as a result of hydrothermal alteration (Baragar et al. 1977; Hart and Staudigel 1978; Richardson et al. 1980; Alt et al. 1986; Alt and Teagle 1999). Much of this carbonate will survive subduction, even in the presence of dehydration and partial melting of the subducting slab (Otto and Wyllie 1993; Yaxley and Green 1994; Yaxley et al. 1994; Molina and Poli 2000; Kerrick and Connolly 2001). Calcite subducted to eclogite facies P–T conditions as part of basaltic oceanic crust will react with garnet to form calcite–dolomite solid solutions. Although the fate of subducted crustal material is a matter of considerable debate, it appears likely that at least a portion of it may ultimately be incorporated into the peridotitic convecting upper mantle, or into mantle plumes, as discrete eclogitic or pyroxenitic bodies (e.g. Hofmann 1997). Their precise form is unknown, but they may exist as elongate streaks with thicknesses of metres to kilometres (Allègre and Turcotte 1986; Christensen and Hofmann 1994). Thus, subduction of altered, carbonated oceanic crust may result in carbonate-bearing eclogitic or pyroxenitic bodies surrounded by peridotite wall rock.

The presence in the upper mantle of carbonate-bearing, recycled oceanic crust is supported by geochemical evidence from a number of sources. Many ocean island basalts (OIBs) exhibit the HIMU signature with radiogenic Pb isotopes, low ϵ_{Nd}, high $^{87}Sr/^{86}Sr$ and high $^{187}Os/^{186}Os$ (e.g. Hauri and Hart 1993; Kogiso et al. 1997; Lassiter and Hauri 1998). These characteristics have most often been interpreted as deriving from ancient oceanic crust in which U/Pb and Th/Pb were elevated due to hydrothermal processes at the mid-ocean ridge or dehydration processes during subduction. This altered crustal material was recycled at convergent margins, sequestered in the mantle for billions of years and finally incorporated in the source regions of some intraplate volcanics (Hofmann and White 1982; Hauri and Hart 1993; Hofmann 1997).

Crustally emplaced carbonatites have very similar isotopic compositions to OIBs, and many also have the HIMU signature (Nelson et al. 1988; Bell 2001; Bell and Tilton 2001). Hoernle et al. (2002) has shown that some carbonatites from oceanic settings have stable and radiogenic isotope signatures similar to HIMU OIBs. They interpreted this in terms of formation of the carbonatites by partial melting of subducted carbonated oceanic crust (now carbonated eclogite), which was recycled back into the mantle 1.6 Ga ago.

Nelson et al. (1988) suggested that the sources of some OIBs may be relatively depleted peridotite refertilised by carbonatite melts. Also, in a study of four metasomatised mantle xenoliths from ocean islands associated with the Samoan and Macdonald hot spots, Hauri et al. (1993) linked metasomatic carbonatite melts and mantle source regions containing an ancient recycled oceanic crustal component. Petrographic and geochemical evidence suggested metasomatism by carbonatite melts of the lithosphere underlying the Macdonald and Samoan hot-spots. The extreme HIMU isotopic signatures present in some of the xenoliths linked their HIMU geochemistry with metasomatic carbonatites derived from ancient, recycled, carbonated oceanic crust.

Thus, it appears that the isotopic compositions of some crustally emplaced carbonatites and mantle metasomatic carbonatites may indicate derivation from carbonate that was formerly part of the oceanic crust and has been recycled back into the mantle at convergent margins.

Important controls on the behaviour of carbonate-bearing eclogite and its partial melts in the peridotitic upper mantle will be the physical properties of the carbonatite liquid, the ambient oxygen fugacity (fO_2) and temperature, and the relative positions in P-T space of the eclogite + CO_2 and peridotite + CO_2 solidii.

Carbonate melts are of very low density and viscosity and, therefore, are expected to segregate from source eclogite at very low melt fractions and to infiltrate surrounding peridotitic wall rock (Hunter and McKenzie 1989; Treiman 1989; Minarik and Watson 1995). Luth (1993) has shown that the lower fO_2 stability limit of carbonate in eclogite at high pressure is defined by the reaction dolomite + 2coesite = diopside + 2diamond + $2O_2$. Importantly, equivalent reactions defining carbonate stability in T-fO_2 space in peridotite assemblages lie at significantly lower fO_2. Therefore, if peridotite and entrained eclogite bodies are at similar ambient fO_2, carbonate will be stable in eclogite and in the surrounding peridotite.

If the eclogite + CO_2 solidus is at lower temperatures than the local peridotite + CO_2 solidus, carbonatitic partial melts segregating from their eclogite source will react and solidify upon percolating into peridotite wall rock. Carbonate will crystallise as dolomite at pressures below the vapour absent reaction dolomite + enstatite = magnesite + diopside, which intersects the peridotite solidus at $\approx$2.5 GPa (Brey et al. 1983). This will be accompanied by increases in whole-rock Ca/Mg and LILE abundances in the peridotite. At pressures above the aforementioned reaction, carbonate will crystallise as magnesite, with a substantial increase in peridotite's modal clinopyroxene/orthopyroxene ratio.

If the eclogite + CO_2 solidus is at higher temperatures than that of peridotite + CO_2, the eclogite-derived carbonatites will remain liquid upon entering the peridotite. The carbonatite melt's composition will adjust to equilibrium with the peridotite, evolving from calcio-dolomitic to more dolomitic compositions (Dalton and Prenall 1998; Wallace and Green 1988), accompanied by increased Ca/Mg in the peridotite, again manifest as increased modal clinopyroxene/orthopyroxene, and as Fe, alkali and LILE enrichment. This enrichment will further locally lower the wall-rock peridotite's solidus. Continued influx of calcio-dolomitic carbonatite may eliminate orthopyroxene in peridotite, replacing it with clinopyroxene. The carbonatite melt will develop lower Fe/Mg, reflecting equilibrium with highly magnesian olivine and pyroxenes in peridotite, rather than higher Fe/Mg eclogitic phases.

The P–T path of the Hawaiian pyrolite + CO_2 solidus has been determined by Falloon and Green (1989), and lies well below the solidus of EC1 (Fig. 9). However, EC1 is a model composition, and natural carbonated eclogite solidi are expected to vary considerably. Higher whole-rock alkali contents will result in lower carbonate solidus temperatures at a given pressure (Jago and Gittins 1991; Yaxley 1999), as also illustrated by the experiments with the more sodic composition EC2. In addition, the amount of carbonate in the source rock may affect solidus temperatures. For a given alkali content, an eclogite with low total carbonate will then have a lower solidus than a similar bulk composition with a higher total carbonate as the alkalis will be more efficiently able to flux melting. Compositions with lower Ca/Mg than EC1 may also crystallise magnesite, rather than dolomitic carbonate leading to different solidus temperatures (Yaxley and Green 1994). These aspects of the melting behaviour of carbonated eclogite and pyroxenite remain to be explored experimentally. Also, natural upper mantle carbonate-bearing eclogite may contain volatiles such as F^- and H_2O, which will also lower carbonate melting temperatures (Jago and Gittins 1991). Therefore, it is expected that discrete carbonate-bearing eclogite bodies entrained in the convecting upper mantle will have a range of solidus temperatures at a given pressure, and that they will in many cases be lower than that of EC1.

The potential temperature (T_p) of ambient convecting upper mantle is generally assumed to be 1,280 °C (McKenzie and Bickle 1988) although it may be as high as 1,430 °C (Green et al. 2001). In the following discussion, we adopt the lower, more conservative estimate of 1,280 °C. If this is correct, P–T conditions in the solid convecting upper mantle are expected to lie close to an adiabat with $T_p = 1{,}280$ °C. At 3.0 GPa the EC1 solidus is ≈180 °C below this adiabat, and at 5.0 GPa it is ≈70 °C below it. If the EC1 solidus is extrapolated to higher pressures it intersects the adiabat at depths corresponding to pressures of 7–8 GPa (point 1 on Fig. 9). Therefore, if discrete bodies of carbonated eclogite are present in peridotite-dominated convecting upper mantle, the carbonate in those with a similar solidus to EC1 may be molten in the upper ≥250 km. If the convecting mantle's potential temperature is higher (Green et al. 2001), or if carbonated eclogite bodies are entrained in hot mantle plumes, or if the solidi of some carbonate eclogite bodies are lower than that of EC1, melting will occur at much greater depths.

At 3.0 GPa, the solidus of EC1 is ≈130 °C above the Hawaiian pyrolite–CO_2 solidus (Falloon and Green 1989, 1990) and ≈300 °C above the Hawaiian pyrolite–CO_2 + H_2O solidus (Wallace and Green 1988). Therefore, carbonate liquids derived from partial melting of

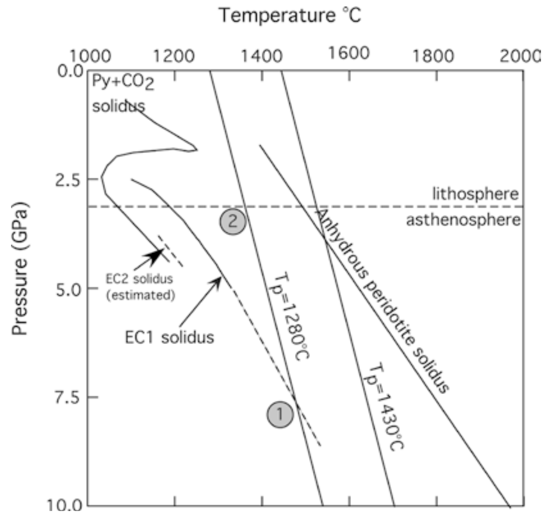

Fig. 9 Pressure–temperature plot showing pyrolite + CO_2 and anhydrous pyrolite solidi (McKenzie and Bickle 1988; Falloon and Green 1989), the EC1 solidus determined in the current experiments and extrapolated to intersect a mantle adiabat with potential temperature (T_p) of 1,280 °C. Also shown is a hotter mantle adiabat ($T_p = 1{,}430$ °C) after Green et al. (2001). The asthenosphere–lithosphere boundary is shown at a representative depth. *Numbered symbols* are explained in the text

many discrete carbonated eclogite bodies in fertile peridotite-dominated upper mantle will remain molten as they infiltrate peridotite wall rock. However, their compositions will change from broadly calcio-dolomitic in equilibrium with eclogitic residue to sodic dolomitic carbonatite (see above). If carbonatite melts continue to ascend through peridotitic wall rock by porous flow they may evolve compositionally away from carbonatite and towards carbonated undersaturated silicate melts such as olivine melilitites or nephelinites, in equilibrium with peridotite, depending on P–T conditions and bulk composition (point 2 on Fig. 9). For this reason, it is unlikely that these primary eclogite-derived carbonatite liquids are ever emplaced into the crust as carbonatites. However, they are likely to have a role in enriching and sometimes carbonating regions of the convecting mantle or lithosphere, which on subsequent melting may produce carbonatites or related carbonated undersaturated silicate liquids.

Conclusions

1. Carbonate-bearing eclogitic assemblages are capable of producing calcio-dolomitic carbonatite liquids at upper mantle pressure–temperature conditions, providing ambient oxygen fugacities are appropriate for carbonate stability.
2. Ca-(Mg + Fe) exchange between garnet and carbonate results in crystallisation of calcite–dolomite solid solution in eclogite at high pressures. As a result, melting relations mainly reflect minimum melting on the calcite–magnesite join.

3. However, Na abundance in the eclogite also has an important effect in lowering solidus temperatures. This is probably controlled by a melting reaction in which jadeite in clinopyroxene and dolomite in carbonate react to produce sodium carbonate and silica in the carbonatitic liquid and increased Tschermak's components in residual clinopyroxene.
4. The solidus temperature of EC1 is higher than that of peridotite–CO_2, meaning that carbonatite melts that segregate from a similar eclogite source and percolate into surrounding peridotite wall rock will remain molten. They will, however, metasomatise the peridotite through which they pass. Natural carbonated eclogites are expected to have a range of solidus temperatures depending on compositional factors, such as Na and CO_2 contents and Ca/Mg ratio. The relative positions in P–T space of carbonated eclogite and peridotite solidii will control the nature of interactions between eclogite-derived carbonatites and peridotite wall rocks.
5. Carbonatite liquids are likely to form from carbonated eclogites at great depths, depending on mantle potential temperature and solidus temperature. Such melts are unlikely to reach the crust or lithosphere unmodified, but may evolve towards carbonated, silica-undersaturated silicate liquids, which could subsequently evolve or unmix to produce carbonatites.

Acknowledgements We gratefully acknowledge the assistance of Thomas Kautz, Daniel Röhnert and Vadim Bulatov (Universität Frankfurt), and Bill Hibberson (ANU) with the experiments, Jan Heliosch (Universität Frankfurt) with sample preparation, and Frank Brink (ANU) with the electron microscopy. This study benefited from discussions with David Green, Jörg Hermann, Andrei Girnis and Thomas Stachel, and the manuscript was improved by careful and constructive reviews from Stephen Foley and Stefano Poli. This project was supported by the Alexander von Humboldt Foundation (GMY), the Deutsche Forschungsgemeinschaft (GPB) and the Australian Research Council (GMY).

References

Allègre CJ, Turcotte DL (1986) Implications of a two-component marble-cake mantle. Nature 323:123–127

Alt JC, Teagle DAH (1999) The uptake of carbon during alteration of ocean crust. Geochim Cosmochim Acta 63:1527–1535

Alt JC, Honnorez J, Laverne C, Emmermann R (1986) Hydrothermal alteration of a 1 km section through the upper oceanic crust, deep sea drilling project hole 504B: mineralogy, chemistry and evolution of sea-water basalt interactions. J Geophys Res 91:10309–10335

Baragar WRA, Plant AG, Pringle GJ, Schau M (1977) Petrology and alteration of selected units of Mid-Atlantic Ridge basalts samples from sites 332 and 335, DSDP. Can J Earth Sci 14:837–874

Bell K (2001) Carbonatites: relationships to mantle plume activity. Geol Soc Am Spec Paper 352:267–290

Bell K, Tilton GR (2001) Nd, Pb and Sr isotopic compositions of East African carbonatites: evidence for mantle mixing and plume inhomogeneity. J Petrol 42:1927–1945

Bell K, Blenkinson J, Cole J, Menagh DP (1982) Evidence from Sr isotopes for long-lived heterogeneities in the upper mantle. Nature 298:251–253

Bose K, Ganguly J (1995) Quartz–coesite transition revisited: reversed experimental determination at 500–1,200 °C and retrieved thermochemical properties. Am Mineral 80:231–238

Brey G, Brice WR, Ellis DJ, Green DH, Harris KL, Ryabchikov ID (1983) Pyroxene–carbonate reactions in the upper mantle. Earth Planet Sci Lett 62:63–74

Brey GP, Weber R, Nickel KG (1990) Calibration of a belt apparatus to 1,800 °C and 6 GPa. J Geophys Res 95:603–615

Byrnes AP, Wyllie PJ (1981) Subsolidus and melting relations for the join $CaCO_3$–$MgCO_3$ at 10 kb. Geochim Cosmochim Acta 45:321–328

Christensen UR, Hofmann AW (1994) Segregation of subducted oceanic crust in the convecting mantle. J Geophys Res 99:19867–19884

Dalton JA, Prenall DC (1998) Carbonatitic melts along the solidus of model lherzolite in the system CaO–MgO–Al_2O_3–SiO_2–CO_2 from 3 to 7 GPa. Contrib Mineral Petrol 131:123–135

Dalton JA, Wood BJ (1993) The compositions of primary carbonate melts and their evolution through wallrock reaction in the mantle. Earth Planet Sci Lett 119:511–525

Deines P (1989) Stable isotope variations in carbonatites. In: Bell, K (ed) Carbonatites: genesis and evolution. Unwin Hyman, London, pp 301–359

Ellis DJ, Green DH (1979) An experimental study of the effect of Ca upon garnet–clinopyroxene Fe–Mg exchange equilibria. Contrib Mineral Petrol 71:13–22

Falloon TJ, Green DH (1989) The solidus of carbonated, fertile peridotite. Earth Planet Sci Lett 94:364–370

Falloon TJ, Green DH (1990) Solidus of carbonated fertile peridotite under fluid-saturated conditions. Geology 18:195–199

Green DH, Falloon TJ, Eggins SM, Yaxley GM (2001) Primary magmas and mantle temperatures. Eur J Mineral 13:437–451

Hart SR, Staudigel H (1978) Oceanic crust: age of hydrothermal alteration. Geophys Res Lett 5:1009–1012

Hauri EH, Hart SR (1993) Re–Os isotope systematics of HIMU and EMII oceanic islands from the south Pacific Ocean. Earth Planet Sci Lett 114:353–371

Hauri EH, Shimuzu N, Dieu JJ, Hart SR (1993) Evidence for hotspot-related carbonatite metasomatism in the oceanic upper mantle. Nature 365:221–227

Hermann J, Rubatto D, Korsakov A, Shatsky VS (2001) Multiple zircon growth during fast exhumation of diamondiferous, deeply subducted continental crust (Kokchetav Massif, Kazakhstan). Contrib Mineral Petrol 141:66–82

Hoernle K, Tilton GR, Le Bas MJ, Duggen S, Garbe-Schönberg D (2002) Geochemistry of oceanic carbonatites compared with continental carbonatites: mantle recycling of oceanic crustal carbonate. Contrib Mineral Petrol 142:520–542

Hofmann AW (1997) Mantle geochemistry: the message from oceanic volcanism. Nature 385:219–229

Hofmann AW, White WM (1982) Mantle plumes from ancient oceanic crust. Earth Planet Sci Lett 57:421–436

Hunter RH, McKenzie D (1989) The equilibrium geometry of carbonate melts in rocks of mantle composition. Earth Planet Sci Lett 92:347–356

Irving A, Wyllie P (1975) Subsolidus and melting relationships for calcite, magnesite and the join $CaCO_3$–$MgCO_3$ to 36 kb. Geochim Cosmochim Acta 39:35–53

Jago BC, Gittins J (1991) The role of fluorine in carbonatite magma evolution. Nature 349:56–58

Kerrick DM, Connolly JAD (2001) Metamorphic devolatilization of subducted oceanic metabasalts: implications for seismicity, arc magmatism and volatile recycling. Earth Planet Sci Lett 189:19–29

Kjarsgaard BA, Hamilton DL (1988) Liquid immiscibility and the origin of alkali-poor carbonatites. Mineral Mag 52:43–55

Kjaarsgaard BA, Hamilton DL (1989) Carbonatite origin and diversity. Nature 338:547–548

Kogiso T, Tatsumi Y, Shimoda G, Barsczus HG (1997) High μ (HIMU) oceanic island basalts in southern Polynesia: new evidence for whole mantle scale recycling of subducted oceanic crust. J Geophys Res 102:8085–8103

Koster van Groos AF, Wyllie PJ (1973) Liquid immiscibility in the join $NaAlSi_3O_8$–$CaAl_2Si_2O_8$–Na_2CO_3–H_2O. Am J Sci 273:465–487

Kwon S-T, Tilton GR, Grünenfelder MH (1989) Lead isotope relationships in carbonatites and alkalic complexes: an overview. In: Bell K (ed) Carbonatites: genesis and evolution. Unwin Hyman, London, pp 360–387

Lassiter JC, Hauri EH (1998) Osmium isotope variations in Hawaiian lavas: evidence for recycled oceanic lithosphere in the Hawaiian plume. Earth Planet Sci Lett 164:483–496

Lee W-J, Wyllie PJ (1996) Liquid immiscibility in the join $NaAlSi_3O_8$–$CaCO_3$ to 2.5 GPa and the origin of calciocarbonatite magmas. J Petrol 37:1125–1152

Lee W-J, Wyllie PJ (1997a) Liquid immiscibility between nephelinite and carbonatite from 1.0 to 2.5 GPa compared with mantle melt compositions. Contrib Mineral Petrol 127:1-16

Lee W-J, Wyllie PJ (1997b) Liquid immiscibility in the join $NaAlSiO_4$–$NaAlSi_3O_8$–$CaCO_3$ at 1 GPa: implications for crustal carbonatites. J Petrol 38:1113–1135

Luth RW (1993) Diamonds, eclogites, and the oxidation state of the Earth's mantle. Science 261:66–68

Luth RW (1995) Experimental determination of the reaction dolomite + 2 coesite = diopside + 2 CO_2 to 6 GPa. Contrib Mineral Petrol 122:152–158

Luth RW (2001) Experimental determination of the reaction aragonite + magnesite = dolomite at 5 to 9 GPa. Contrib Mineral Petrol 141:222–232

McKenzie D, Bickle MJ (1988) The volume and composition of melt generated by extension of the lithosphere. J Petrol 29:625–679

Minarik WG, Watson EB (1995) Interconnectivity of carbonate melt at low melt fraction. Earth Planet Sci Lett 133:423–437

Molina JF, Poli S (2000) Carbonate stability and fluid composition in subducted oceanic crust: an experimental study on H_2O–CO_2-bearing basalts. Earth Planet Sci Lett 176:295–310

Nelson DR, Chivas AR, Chappell BW, McCulloch MT (1988) Geochemical and isotopic systematics in carbonatites and implications for the evolution of ocean-island sources. Geochim Cosmochim Acta 52:1–17

Otto JW, Wyllie PJ (1993) Relationships between silicate melts and carbonate-precipitating melt in CaO–MgO–SiO_2–CO_2–H_2O at 2 kbar. Mineral Petrol 48:343–365

Richardson SH, Hart SR, Staudigel H (1980) Vein mineral ages of old oceanic crust. J Geophys Res 85:7195–7200

Rudnick RL, McDonough WF, Chappell BW (1993) Carbonatite metasomatism in the northern Tanzanian mantle: petrographic and geochemical characteristics. Earth Planet Sci Lett 114:463–476

Sweeney RJ (1994) Carbonatite melt compositions in the Earth's mantle. Earth Planet Sci Lett 128:259–270

Thibault Y, Edgar AD, Lloyd FE (1992) Experimental investigation of melts from a carbonated phlogopite lherzolite: implications for metasomatism in the continental lithospheric mantle. Am Mineral 77:784–794

Tilton GR, Bell K (1994) Sr–Nd–Pb isotope relationships in late Archean carbonatites and alkaline complexes: applications to the geochemical evolution of the mantle. Geochim Cosmochim Acta 58:578–583

Treiman AH (1989) Carbonatite magmas: properties and processes. In: Bell K (ed) Carbonatites: genesis and evolution. Unwin Hyman, London, pp 89–104

Treiman AH, Essene EJ (1983) Mantle eclogite and carbonate as sources of sodic carbonatites and alkalic magmas. Nature 302:700–703

Veksler IV, Nielsen TFD, Sokolov SV (1998) Mineralogy of crystallized melt inclusions from Gardiner and Kovdor ultramafic alkaline complexes: implications for carbonatite petrogenesis. J Petrol 39:2015–2031

Wallace M, Green DH (1988) An experimental determination of primary carbonatite composition. Nature 335:343–345

Wyllie PJ, Huang W-L (1975) Influence of mantle CO_2 in the generation of carbonatites and kimberlites. Nature 257:297–299

Wyllie P, Huang W-L (1976) Carbonation and melting reactions in the system CaO–MgO–SiO_2–CO_2 at mantle pressures with geophysical and petrological applications. Contrib Mineral Petrol 54:79–107

Yaxley GM (1999) Phase relations of carbonated eclogite under upper mantle PT conditions — implications for carbonatite petrogenesis. Proceedings of the 7th International Kimberlite Conference, Cape Town, vol 2, pp 933–939

Yaxley GM, Green DH (1994) Experimental demonstration of refractory carbonate-bearing eclogite and siliceous melt in the subduction regime. Earth Planet Sci Lett 128:313–325

Yaxley GM, Crawford AJ, Green DH (1991) Evidence for carbonatite metasomatism in spinel peridotite xenoliths from western Victoria, Australia. Earth Planet Sci Lett 107:305–317

Yaxley GM, Green DH, Klápová H (1994) The refractory nature of carbonate during partial melting of eclogite: evidence from high pressure experiments and natural carbonate-bearing eclogites. Mineral Mag 58A:996–997